Chaos, Solitons and Fractals 185 (2024) 115089

Contents lists available at ScienceDirect

Chaos, Solitons and Fractals

journal homepage: www.elsevier.com/locate/chaos

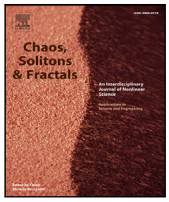

# A multifractal approach to understanding Forbush Decrease events: Correlations with geomagnetic storms and space weather phenomena

D. Sierra-Porta

*Facultad de Ciencias Básicas, Universidad Tecnológica de Bolívar, Parque Industrial y Tecnológico Carlos Vélez Pombo Km 1 Vía Turbaco, Cartagena de Indias, 130010, Bolívar, Colombia*

ARTICLE INFO

*Keywords:*
Multifractal behavior
Forbush decrease
Space weather
Cosmic rays

ABSTRACT

The Forbush decrease phenomenon has significant impacts on several environmental conditions, including interference in radio communications, satellite navigation systems, and the health of astronauts in space, among others. It is characterized by a temporary and noticeable reduction in the observed flux of galactic cosmic rays recorded at the Earth's surface. This decrease occurs due to the modulation of cosmic rays through their interaction with shock waves generated by coronal mass ejections. As these shock waves traverse the interplanetary medium, which includes the solar wind and galactic cosmic rays, they exert compression forces on the cosmic ray flux, leading to a reduction in observed flux levels at Earth. This study investigates Forbush Decrease events across different solar cycles and explores their correlation with geomagnetic storm conditions using multifractal detrended fluctuation analysis. The findings indicate variations in the multifractal spectra for series under different geomagnetic storm conditions compared to the full Forbush decrease series. Moreover, it is observed that the amplitude of the multifractal spectrum is greater in the series that include events with a maximum $Kp$ index exceeding 6, suggesting a significant influence of geomagnetic storm conditions on the fractality and variability of Forbush Decrease magnitudes.

## 1. Introduction

A Forbush decrease (FD) is an observed phenomenon in the activity of charged particles, particularly galactic cosmic rays from outer space. This event occurs due to a coronal mass ejection (CME) on the Sun, generating a shock wave that propagates through the interplanetary medium, including the solar wind and galactic cosmic rays [1–3]. Coined by physicist Scott E. Forbush in the 1930s [4–6], a Forbush decrease is characterized by a reduction in the flux of cosmic rays observed at Earth. The shock wave resulting from a CME compresses cosmic rays, leading to a decrease in their observed flux at Earth [7–9].

This is essentially a heliospheric process. This decrease occurs due to the modulation of cosmic rays by the shock wave associated with the CME. The effect of the FD can last from several hours to several days [10,11], depending on the speed of the shock wave [12,13] and the characteristics of the CME [14,15].

There are two types of precursors to the cosmic ray flux reduction effect associated with two types of interplanetary distortions. The first is caused by precisely CMEs that result in peaks of geomagnetic activity observed with high values of $Kp$ and Dst (Disturbance Storm Time) indices [16–18]. The second effect has to do mainly with distortions in the heliospheric current sheet (HCS) [19,20], a disk-shaped structure that extends throughout the solar system. It is formed due to the Sun's magnetic field configuration, which is dipole-shaped. The solar magnetic field is generated by dynamic activity in the interior of the Sun and extends out into interplanetary space and is produced by the differential rotation of the Sun and creates a complex and dynamic structure in the magnetic field of the solar system. This results in variations in the strength and direction of the magnetic field in different regions of interplanetary space.

The $Kp$ [21,22] and Dst [23] indices are fundamental tools in the investigation of geomagnetic activity and its effects on the Earth's magnetosphere. The Planetary $Kp$ Index is a measure that quantifies the global geomagnetic disturbance caused by solar storms and other disturbances in the solar wind. It is calculated from observations of the horizontal component of the magnetic field at ground-based stations distributed around the world. These stations measure variations in the magnetic field, and the data are used to determine the value of the $Kp$ index on a scale ranging from 0 (minimum geomagnetic activity) to 9 (maximum geomagnetic activity). The $Kp$ Index is updated regularly and provides real-time information on geomagnetic conditions.

On the other hand, the Dst Index is an indicator that assesses the impact of geomagnetic storms on Earth's magnetosphere. It is derived from measurements of the north–south component of the magnetic field

*E-mail address:* dporta@utb.edu.co.

https://doi.org/10.1016/j.chaos.2024.115089
Received 24 June 2023; Received in revised form 17 January 2024; Accepted 28 May 2024
Available online 4 June 2024

at a network of ground stations distributed around the world. The Dst Index measures the intensity of the geomagnetic storm and quantifies the reduction in electric current within Earth's magnetosphere during these events. When a solar storm or coronal mass ejection from the Sun reaches Earth, it can induce electrical currents within the magnetosphere, subsequently affecting power grids, communication systems, and navigation systems. The Dst index serves as a critical tool for monitoring and predicting these adverse effects.

These indices are crucial measurements for quantifying and monitoring geomagnetic activity, offering invaluable insights into comprehending and mitigating the effects of solar storms on Earth. Scientific institutions and space agencies worldwide conduct these measurements, and their significance resides in their capacity to forecast and manage the detrimental consequences of solar activity on terrestrial technology and infrastructure.

FDs are frequently linked to a sudden increase in geomagnetic activity resulting from the arrival of solar particles. As a result, observing a rise in the $Kp$ index could serve as an indication that an FD is underway or has recently occurred. When an FD occurs, there is typically a noteworthy reduction in the Dst index value. This reduction is attributable to the reduction in electric current within the magnetosphere due to the interception of solar particles. Consequently, an FD event is manifested as a decrease in the Dst index.

The heliospheric current sheet (HCS) is closely related to solar activity, including coronal mass ejections (CMEs) and solar storms. During CME events, the interaction between the HCS and CMEs can lead to geomagnetic storms on Earth, which can disrupt power grids, communications, and navigation systems. Therefore, the FD phenomenon can have significant impacts on various aspects, such as interference in radio communications and satellite navigation systems, as well as on the health of astronauts in space.

Furthermore, there are two types of interplanetary geomagnetic distortions: sporadic and recurrent [17,24–26]. Sporadic distortions are single, unpredictable events that occur sporadically in interplanetary space as a result of solar phenomena, such as CMEs. In contrast, recurrent geomagnetic distortions are events that occur periodically and predictably due to the Sun's rotation. These distortions occur as the Earth passes through the heliospheric current sheet, resulting in a distortion of the interplanetary magnetic field. This, in turn, affects the Earth's magnetosphere and can generate recurrent geomagnetic disturbances. Recurrent geomagnetic storms are most common during seasonal changes and are known as recurrent geomagnetic storms.

In a previous study [27] the authors have examined daily FD data spanning from 1967 to 2003, focusing on the rapid decay of galactic cosmic ray intensity preceding CMEs. After applying data filtering techniques, the Hurst Exponent and Fractal Dimension are calculated, using the Finite Variance Scaling Method and Higuchi's Method separately on the processed data, revealing that the data exhibit antipersistent behavior, indicating a short memory process. These findings suggest that cosmic ray intensity variations do not retain significant memory of past events, posing challenges for prediction and indicating the likelihood of complex multiperiodic patterns. Detection of underlying periodicities in Forbush decay phenomena remains a research challenge for the future.

Another study [28] investigates space weather events during solar cycle 24 by analyzing cosmic ray flux data measured by neutron monitors. The research focuses on periods of halo CMEs and sudden storm commencements. The findings reveal that the fractal dimension, skewness, and kurtosis of cosmic ray intensity change significantly during these events. Additionally, the study links these space weather indicators to electrical grid failures in southern Poland during the same time intervals, suggesting that statistical properties of cosmic ray intensity and solar/geomagnetic parameters can serve as reliable indicators of space weather events. The study also suggests a solar cycle dependence in the occurrence of electrical grid failures, with more failures observed during the solar maximum in 2014 compared to the solar minimum in 2010. Furthermore, an increase in grid failures is noted around FDs, SSCs, and elevated $Kp$ index values, as well as one day after fast halo CMEs occur.

More recently [29] focuses on forecasting extreme space weather events based on fluctuations in high-energy cosmic rays. Such events involve the formation of large fluxes of storm particles preceding shock waves reaching Earth's orbit, posing significant threats to life-support systems in the upper atmosphere and in space. The research demonstrates, applying the method of probabilistic identification of the transient regime, the prediction of these storm particles accelerated by shock waves using measurements from the ACE spacecraft in the United States, with a forecast reliability of $P \geq 80\%$. The study's key conclusions highlight the nonlocal behavior of cosmic rays in fractal magnetic fields and explores the prediction of dangerous space weather events by studying cosmic ray fluctuations and sheds light on the nonlocal behavior of cosmic rays in the presence of fractal magnetic fields, with practical applications in forecasting and understanding extreme space weather events.

In this paper, we employ an unconventional but increasingly important methodology based on a comprehensive review of the existing literature to investigate the series of FD events. Our main objective is to examine the presence of fractal patterns in the signals and magnitudes associated with these FD events, utilizing observational databases. Additionally, we aim to analyze the temporal evolution of these signals by utilizing ranges of geomagnetic distortion indices induced by CMEs, with a specific focus on the $Kp$ index, which has demonstrated a correlation with the magnitude of the FD effect [19,30–32].

To assess fractality, we employ the Multifractal Detrended Fluctuation Analysis (MFDFA) technique, which has been widely used in diverse contexts to analyze time series signals. This methodology has been previously applied to examine various phenomena, such as assessing the characteristics of rainfall time series [33–35], analyzing the scaling behaviors of fractal structures in financial time series fluctuations [36–38], studying energy stocks [39,40], particulate matter and atmospheric variables [41], analyzing traffic time series [42,43], and investigating sunspot series in the context of space weather [44,45], as well as cosmic ray data and space weather data [46–51].

In the realm of geomagnetic storm research, time series analysis plays a crucial role in unraveling the intricate dynamics of these events and their connection to solar activity. However, the inherent variability in the magnitudes of geomagnetic storms has long challenged attempts to accurately model and predict these phenomena. In this context, the application of MFDFA has emerged as a powerful tool that enables a more profound and comprehensive exploration of the intrinsic structure and long-range dependence within time series data.

This study focuses on the application of MFDFA to geomagnetic storm magnitude time series, with the aim of unveiling hidden patterns and multifractal behaviors that may not be evident at first glance. The significance of this research lies in its capacity to shed light on the variability and unpredictability of these events, which has substantial implications for predicting and mitigating the impacts of geomagnetic storms on our technological infrastructure and critical communication systems. By gaining a better understanding of the fractal nature of these time series, we are one step closer to developing more accurate models and early warning strategies that can contribute to safeguarding our systems and services against the rigors of outer space.

## 2. Methods and data

### 2.1. Database

The present research article is based on the analysis of a compiled database of FD phenomena obtained from the Izmiran Space Science Research Institute website (http://spaceweather.izmiran.ru/eng/dbs.html). The database encompasses a comprehensive collection of items that capture and describe recorded FD events in detail. These elements

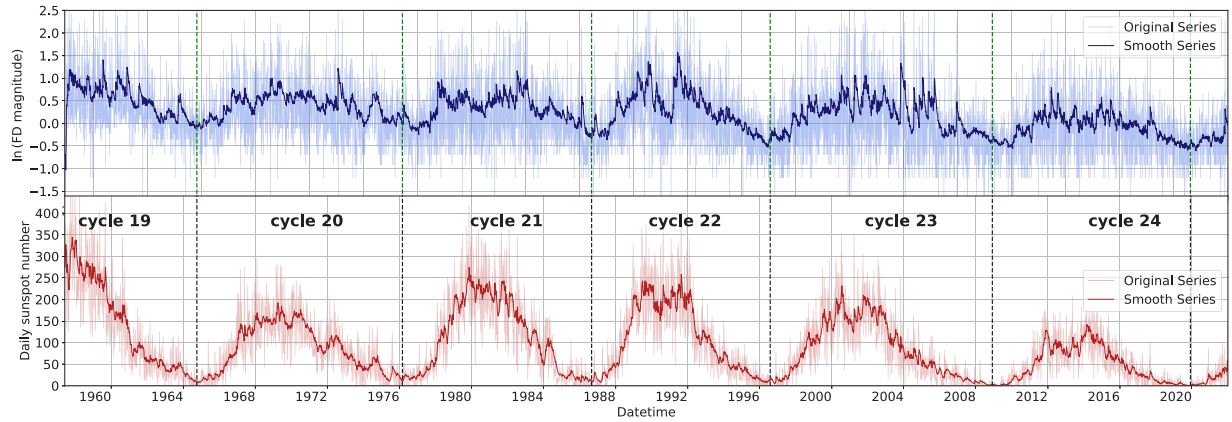


**Fig. 1.** Temporal behavior from June 6, 1957 to December 30, 2021 of the magnitude of the FD events and their relationship in the 5 solar cycles considered. The series exhibits a slightly seasonal behavior.

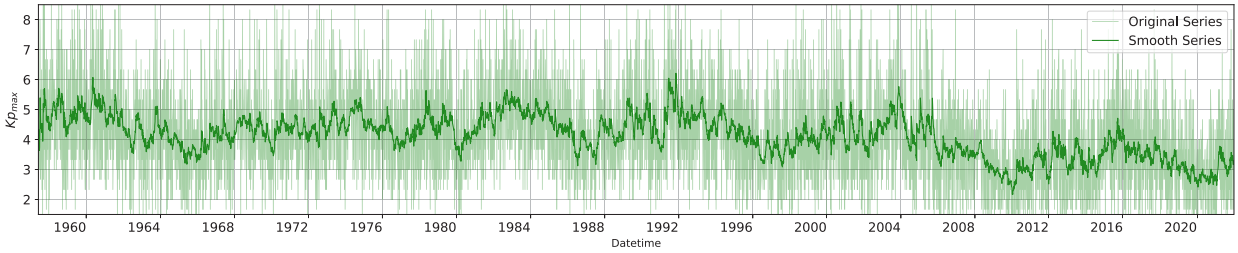


**Fig. 2.** Temporal behavior from June 6, 1957 to December 30, 2021 of the $Kp$ index maximum recorded for the events in Fig. 1.

include, the start and end dates and times of events, maximum decrease amplitude, total duration, solar wind speed, solar wind density, geomagnetic $Kp$ index, interplanetary magnetic field strength, as well as several parameters related to charged particles, such as energy, flux, and energy flux of protons and electrons. A complete description of the measured parameters can be found in the document titled "Full List of Parameters" available at http://spaceweather.izmiran.ru/dbs/fds/full-list-parameters-eng.pdf. This database serves as a valuable source of information for conducting a detailed analysis of FD phenomena and their relationship with the corresponding space–time conditions.

This comprehensive database contain a total of 8216 records of FD events, compiled over a period spanning from June 6, 1957, to December 30, 2021. It provides valuable information on FD events over more than six decades, enabling a long-term analysis of these phenomena. Furthermore, a significant connection will be established between these events and the solar cycles from cycle 19 to 25, with cycle 25 still ongoing (https://en.wikipedia.org/wiki/List_of_solar_cycles). This allows for an examination of the relationship between FD events and the solar activity throughout multiple solar cycles, providing insights into the long-term variations and trends in FD occurrences.

Fig. 1 illustrates the variability and evolution of the magnitude of FD events, specifically for particles with a 10 GV rigidity that have been corrected for magnetospheric effects using the Dst-index. The figure compares the behavior of FD events in relation to solar activity, as indicated by the number of sunspots observed during each of the considered solar cycles.

Furthermore, Fig. 2 displays the behavior of the maximum $Kp$ index recorded for each FD event. The $Kp$ index serves as an indicator of geomagnetic activity associated with the events.

An analysis of the recorded FD events reveals that the most common type of onset is Type 9, which corresponds to the absence of both an interplanetary shock wave and a substorm current (SSC). This type represents the majority of the recorded events, totaling 6363 occurrences. The second most common type involves both an interplanetary shock wave and an SSC, with a count of 1537 events. Type 3, characterized by a weak SSC, follows in third place with 257 events. These counts provide insights into the relative distribution of different types of onset in the analyzed dataset. It is noteworthy that approximately 93% of the events are caused by ejections from active regions accompanied by solar flares or solar filament eruptions from regions beyond the sunspot groups.

In addition to analyzing the time series of FD magnitudes within each solar cycle (filtered by dates), a new dataset was created by filtering the time series based on the geomagnetic storm condition, specifically using the $Kp$ index. Table 1 presents some basic descriptive statistics for this classification. The separation of the dataset based on the geomagnetic activity index is justified due to the observed relationship between this variable ($Kp$ maximum index) and the magnitude of the FD events.

### 2.2. Multifractal detrented fluctuation analysis

The MFDFA [52] which is a generalization of Detrended Fluctuation Analysis (DFA) method [53,54], is a technique used in the field of physics and statistics to study complex and turbulent systems. This approach is based on fractal theory and is applied to signals or data sets that exhibit multifractal behavior, i.e., they exhibit variability on different spatial or temporal scales.

MFDFA is used to characterize the structure and organization of fluctuations in a particular system. Unlike traditional methods that focus on the analysis of single scales, this approach examines how fluctuations vary over different ranges of scales. To do this, functions called detrended fluctuation functions are used that capture the distribution of fluctuations at different levels of detail.

This method makes it possible to quantify the heterogeneity and internal complexity of the systems studied. It provides information on the presence of autoaffine structures, autocorrelations and other characteristic patterns that may not be captured by traditional techniques. Multifractal analysis of detrended fluctuations has been applied in a wide range of disciplines, such as fluid physics, economics, geophysics

**Table 1**
Basic statistics of the time series considered in this study. There are two types of separations of the series we make here: one in terms of solar cycles (date separation) and one in terms of geomagnetic activity conditions.

| Time series | Count | Mean | Std | Min | $Q_1$ | $Q_2$ | $Q_3$ | Max | Skewness | Kurtosis |
|---|---|---|---|---|---|---|---|---|---|---|
| All cycles | 8211 | 1.4 | 1.5 | 0.0 | 0.6 | 1.0 | 1.5 | 28.0 | 5.8 | 56.8 |
| Cycle 19 | 965 | 1.8 | 1.9 | 0.0 | 1.0 | 1.3 | 1.9 | 19.3 | 4.4 | 26.8 |
| Cycle 20 | 1211 | 1.5 | 1.4 | 0.0 | 0.8 | 1.1 | 1.8 | 25.4 | 5.9 | 73.9 |
| Cycle 21 | 1365 | 1.5 | 1.5 | 0.2 | 0.7 | 1.0 | 1.6 | 22.7 | 5.5 | 54.8 |
| Cycle 22 | 1313 | 1.5 | 1.8 | 0.1 | 0.7 | 1.0 | 1.7 | 23.4 | 5.9 | 51.7 |
| Cycle 23 | 1601 | 1.4 | 1.7 | 0.0 | 0.6 | 0.9 | 1.4 | 28.0 | 5.8 | 56.5 |
| Cycle 24 | 1483 | 1.0 | 0.9 | 0.1 | 0.5 | 0.7 | 1.1 | 11.2 | 4.3 | 30.4 |
| Cycle 25 | 275 | 0.7 | 0.6 | 0.2 | 0.5 | 0.6 | 0.9 | 9.8 | 10.5 | 145.8 |
| All cycles, $Kp = [0, 3]$ | 2190.0 | 0.8 | 0.5 | 0.1 | 0.5 | 0.7 | 0.9 | 4.1 | 2.3 | 7.5 |
| All cycles, $Kp = [3, 6]$ | 5839.0 | 1.3 | 0.9 | 0.0 | 0.7 | 1.0 | 1.5 | 15.2 | 3.3 | 20.8 |
| All cycles, $Kp = [6, 9]$ | 1095.0 | 3.2 | 3.1 | 0.0 | 1.3 | 2.2 | 4.0 | 28.0 | 3.1 | 14.4 |

and biology, to better understand the complex processes occurring in these systems and their behavior at different scales.

The technique is divided into 5 or fewer steps depending on how you apply the analysis algorithm, which are described in the article by Kantelhardt et al. [52].

The steps followed to apply the methods are as follows. Assuming we have a dataset time series with points $y_i$ for stamps $x_i$ $(i = 1, \dots, N)$, we construct the fluctuation or variation profile of the series $y(i)$ such that

$$y(i) = \sum_{k=1}^{i} \left( x_k - \bar{x}_k \right). \tag{1}$$

The profile is divided into $N_s = int$ (N/s) non-overlapping segments of equal length $s$ from left to right, where the number of segments is determined by dividing the length of the data by the scale. If the data length $N$ is not an exact multiple of the scale $s$, resulting in leftover data at the ends, the procedure is repeated from the opposite end. As a result, there are a total of twice the number of segments. The main objective of this step is to establish the variability of the series for different scales and to determine the fluctuations in the behavior of the series. In addition, this step removes the behavior and seasonal component of the series if any.

Next, the local trend of each of the $2N_s$ segments is calculated by a least squares fit $y_s^{fit}$. Then the variance is determined by the relation:

$$F^2(n, s) = \sum_{i=1}^{s} \frac{[y((n-1)s + i) - y_n^{fit}(i)]^2}{s}, \tag{2}$$

for $n = 1, \dots, N_s$, or

$$F^2(n, s) = \sum_{i=1}^{s} \frac{[y(N - (n - N_s)s + i) - y_n^{fit}(i)]^2}{s}, \tag{3}$$

for $n = N_s + 1, \dots, 2N_s$. Such a polynomial fit can be linear, quadratic, cubic or higher. Thus this technique is often referred to as MFDFA$m$, where $m$ is the order of the polynomial used in the trending process. Averaging over all segments we obtain the fluctuation function of order $q$, given by:

$$F(s) = \left[ \frac{1}{2N_s} \sum_{n=1}^{2N_s} F^2(n, s)^{q/2} \right]^{1/q}. \tag{4}$$

Finally, the scaling law of the participation function is determined by analyzing the log–log plot of $F_q(s)$ versus $s$ for each value of $q$.

$$F_q(s) \approx s^{H(q)}, \tag{5}$$

where $H(q)$ is known as the generalized Hurst exponent.

The value of $H$ can indicate whether a process is persistent or antipersistent: if $0 \leq H \leq 0.5$ indicates antipersistence. The process under study is antipersistent and tends to decrease (increase) after a previous increase (decrease). An antipersistent process appears very noisy; if $H = 0.5$ corresponds to uncorrelated process; if $0.5 < H \leq 1.0$ for persistence. If a process has been increasing (decreasing) for a period $T$, then it is expected to continue increasing (decreasing) for a similar period. Persistent processes exhibit long-range correlations and show relatively little noise; and finally if $H > 1.0$ is a non-stationary process, stronger long-range correlations are present.

In other words, persistent or antipersistent behavior ultimately measures whether the series can be understood as behavior that can be predicted or not. This is particularly important in time series processes when one wants to make or study the possibility of forecasting at different scales. A series may have a good prognostic scenario at some time scales but at some other time scales it may be considered rather chaotic behavior. If $H(q)$ is approximately constant for all values of $q$, the time series is said to be monofractal, i.e., it exhibits the same behavior at all scales. If $H(q)$ varies significantly, the time series is multifractal, with different scales at different scales. The different scale values are best described by the multifractal spectrum, defined as

$$f(\alpha) = q[\alpha - H(q)] + 1, \tag{6}$$

where $\alpha = H(q) + q\frac{dH(q)}{dq}$. The spectrum is concave downward, and the wider it is, the more multifractal the time series is.

Essentially, $f(\alpha)$ is the dimensionality of the points with point dimensionality $\alpha$, while the latter denotes the intensity of the singularity, or in other words, the power of the multifractality and is sometimes called the Hölder exponent. Another way to relate each of the singularity measures of the series in a more compact way is by means of a Legendre transform

$$q = \frac{df(\alpha)}{d\alpha}, \quad \tau(q) = q\alpha - f(\alpha). \tag{7}$$

When only one Hölder exponent is present, this usually indicates monofractality, whereas in the multifractal case, different parts of the data structure are characterized by different values of $f(\alpha)$, producing a spectrum of $f(\alpha)$ for different values of $f(\alpha)$. Both $H(q)$, $\tau$ and $f(\alpha)$ ultimately determine not only the scaling properties of the series under consideration but also help to discriminate between different processes with fractal characteristics or not, or in other words, processes that tend to be quite regular or recursive, or processes that tend to be chaotic and out of the normal trend.

### 2.3. Multifractal Detrended Cross-Correlation Analysis (MF-DCCA)

In order to complement and corroborate the results obtained using MFDFA, the Multifractal Detrended Cross-Correlation Analysis (MFDCCA) technique was implemented. In order to uncover the multifractal characteristics of two cross-correlated non-stationary signals, Zhou (2008) [55] (also at [56–58]) introduced the multifractal detrended cross-correlation analysis (MFDCCA, also known as MF-DXA), which integrates the MFDFA and DCCA methodologies. This methodology is presented as a natural extension of MFDFA, adapted to study the multifractal relationship between two time series. Unlike MFDFA, which evaluates the internal self-similarity of a single time series, MFDCCA allows us to analyze the cross-similarity relationship between two time series simultaneously.

In the context of our study, MFDCCA proves to be an essential tool to explore the multifractal correlations between the intensities of Forbush events and the $Kp_{max}$ index. The application of this technique has provided a unique perspective on the nature of the relationships between the studied variables, revealing antipersistent behaviors on all the analyzed time scales.

The complementarity between MFDFA and MFDCCA has allowed a more comprehensive characterization of the multifractal properties of Forbush events under different geomagnetic distortion conditions. This comprehensive approach strengthens the validity and reliability of our conclusions, offering a more complete view of the complexity inherent in the dynamics of solar geostorms.

### 2.4. Generalized Hurst Exponent (GHE) approach

The Generalized Hurst Exponent (GHE) approach [59–61] is a mathematical method employed for the characterization of long-range dependence and fractal properties in time series data. This approach extends the classical notion of the Hurst exponent to accommodate multifractal and non-stationary signals. The GHE is particularly valuable when assessing the scale-invariant behavior of complex systems exhibiting diverse patterns of self-similarity across various temporal scales.

Mathematically, the GHE is defined as follows:

$$H(q) = \lim_{\Delta t \to 0} \frac{1}{q} \log \left[ \frac{1}{N} \sum_{i=1}^{N} \left( \frac{X(i+\Delta t)}{X(i)} \right)^{q} \right] \tag{8}$$

Here, $H(q)$ represents the generalized Hurst exponent for a given order $q$. $\Delta t$ denotes the time lag, $N$ is the total number of data points in the time series, and $X(i)$ represents the value of the time series at time point $i$. The exponent $q$ allows for the exploration of different scaling behaviors within the data.

The calculation involves evaluating the average over all possible increments in the time series at varying time lags. The logarithmic term captures the scaling behavior, and the limit as $\Delta t$ approaches zero ensures the convergence of the exponent. Notably, different values of $q$ provide insights into the multifractal nature of the time series; positive values reveal persistent behavior, while negative values indicate anti-persistent behavior.

The GHE approach proves advantageous in scenarios where the traditional Hurst exponent falls short, especially in capturing the intricate dynamics of multifractal systems. By introducing the parameter $q$, the GHE allows for a more nuanced analysis of the scaling properties, enhancing ability to discern the underlying complexity in time series exhibiting multifractal characteristics.

In the context of our study, the GHE serves as a powerful tool to MFDFA, providing a more comprehensive understanding of the fractal and chaotic nature of Forbush decrease events under various geomagnetic distortion conditions.

## 3. Results and discussions

Below, the results of the time series analysis for the magnitude of FD across different solar cycles using the MFDFA method are presented. The first section presents the results for FD magnitudes across all solar cycles, while the second section describes the outcomes of the same magnitudes for the complete historical series of solar cycles, but disaggregated by the range of $Kp_{max}$ index. This division is intended to assess the existing multifractality for both more extreme (severe geomagnetic conditions) and less extreme events (quiet conditions).

### 3.1. Forbush decrease study in different solar cycles

For the analysis of the magnitude series of FD events, we considered a comprehensive dataset comprising 8216 events recorded from the beginning of 1957 to the end of 2021, concerning seven solar cycles including the actual in course cycle. To account for the regular and seasonal behavior of solar activity, particularly in terms of sunspots, we created subsets of data corresponding to each individual solar cycle. In total, seven cycles were included in the analysis, starting from cycle 19 (which start in 1954) and continuing to the present solar cycle 25, which is currently ongoing and has not yet reached its maximum.

Fig. 3 shows the behavior of the amplitude fluctuations $(y_i - \bar{y}_i)$ of FD intensity time series over several solar cycles. The non-continuous red line represents the mean value of the amplitudes in the observed time range in each of the solar cycles, on the X-axis corresponds to the corresponding time stamp. Since the solar cycles do not have the same duration, this time stamp may vary in each cycle.

Given the challenges in studying geomagnetic storms and solar-related indices, we use statistical tools like Probability Density Functions (PDFs) to understand these dynamic phenomena. Two important statistical parameters we use are skewness and kurtosis. Kurtosis helps us measure how irregular the data is and it shapes the PDFs. We calculate kurtosis using $\langle v_s^4 \rangle / \langle v_s^2 \rangle^2$, and skewness as $\langle v_s^3 \rangle / \langle v_s^2 \rangle^{3/2}$, where $s$ represents the increment scale and $v_s(x) = v(x+s) - v(x)$, in this case for the fluctuation function in detrended decomposition.

In Fig. 4, we show the kurtosis and skewness values for fluctuations in our time series data, covering all solar cycles. We then calculated the kurtosis parameter using the equations mentioned earlier, with 30 different increment scales $s$ for the original time series. What we found is that as we decrease the $s$ increments, the level of irregularity in the data increases across all time series. As $s$ gets closer to zero, the kurtosis parameter shows a more or less linear growth pattern, reaching its highest values in the time series of cycles 20, 21, and 25. Furthermore, we observe that all time series exhibit a similar pattern at larger scales, with constant kurtosis values for specific $s$ intervals, though there are some differences between cycles 20 and 25.

For the application of Multifractal Detrended Fluctuation Analysis (MFDFA) to the FD event magnitudes, we used a range of the $q$ parameter, which measures the intensity of fluctuations in the fluctuation function, such that $-5 \leq q \leq 5$. We partitioned the observation windows into intervals ranging from 5 days to 12 years, roughly corresponding to one solar cycle. The parameter $n$ (in Eq. (4)), determining the sizes of the partition windows for the analyzed series, ranged from 5 to len(data)/5. For the polynomial fits within each partition, we employed fifth-order functions, i.e., polynomials of order 5.

The behavior of the fluctuation function can be observed graphically in Fig. 5, representing the observation window size interval (scale) for various fluctuation order values of $q$.

As expected, for the magnitudes of FD events, larger window sizes correspond to larger fluctuations, while smaller time scales exhibit smaller variations. Across all parameter values of $q$, and for all cycles as well as the full 65-year series, the fluctuation function demonstrates multifractal behavior at different observation scales, scaling as $n^H$, where $H$ denotes the Hurst exponent. The Hurst exponent is not constant for all the studied series.

The slightly more erratic behavior observed in the 25th (current) cycle can be attributed to the fact that this cycle is still ongoing and has not yet reached its maximum. Consequently, the size of this series is at most half the size of the previous cycles. Variations are noticeable not only in the complete 65-year FD series but also across all solar cycles. Despite the distinct amplitudes of solar activity in each cycle, there is no substantial evidence indicating significant differences in the fluctuations among the considered series. A comprehensive cross-correlation study between the magnitude of FD events and solar activity could further corroborate this finding, but it is beyond the scope of this study and could be pursued in future dedicated research.

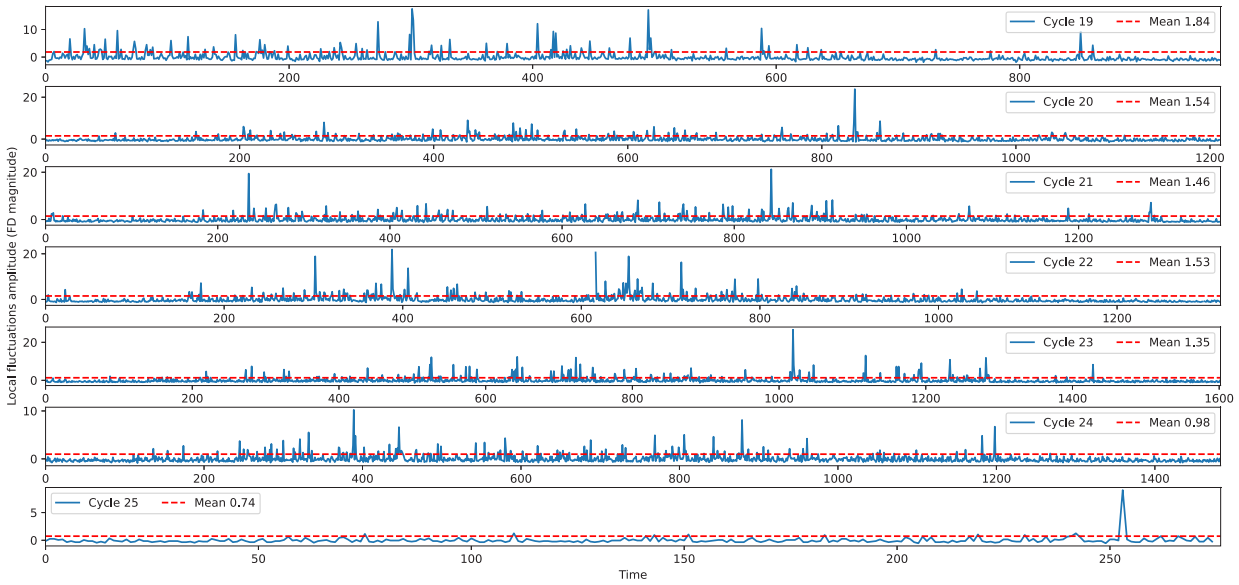


**Fig. 3.** Plots of local fluctuations amplitude for the FD magnitude considered in this study for several solar cycles. Due the solar cycles have different duration, not all have the same time stamp. Evolution for the complete time series is shown in Fig. 1. The dashed lines represent the average in the time interval for each cycle. (For interpretation of the references to color in this figure legend, the reader is referred to the web version of this article.)

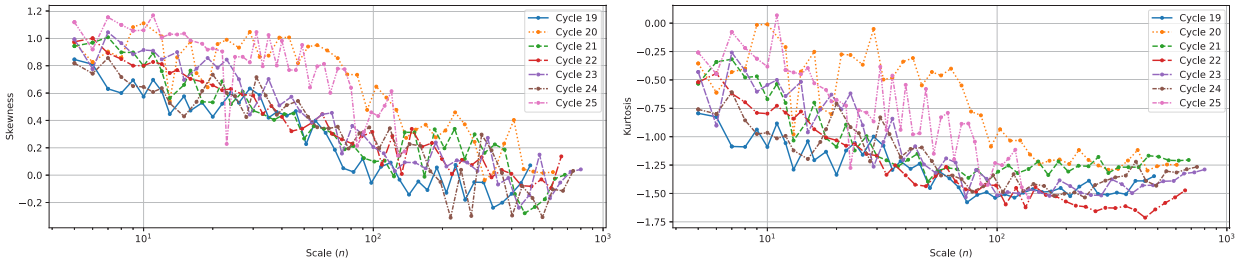


**Fig. 4.** Kurtosis and skewness parameter calculated in 30 increment scales to time-series for several solar cycles.

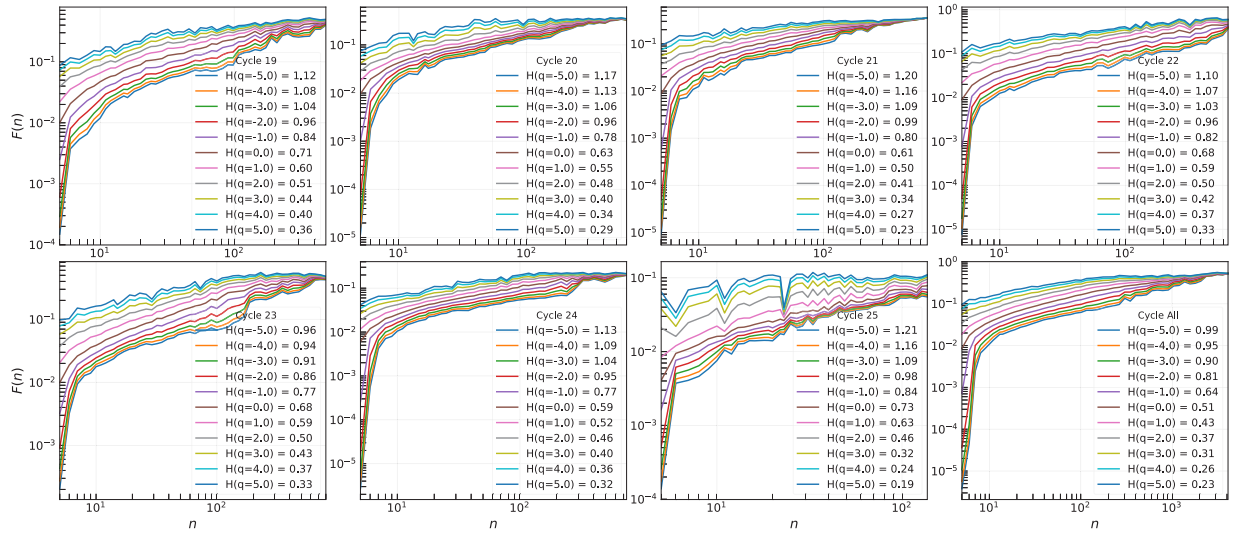


**Fig. 5.** Fluctuation function for several values of the order $q$. Fluctuation function exhibit multifractal behavior with scaling properties.

Based on the maximum observation window sizes considered and the application of the MFDFA method to the analyzed series, it is observed that the scaling properties are most accurately established in the interval $20 \leq n \leq 3000$. Consequently, the fitting is performed within this interval to determine the Hurst exponent for all the series under investigation. Furthermore, it is evident that the Hurst exponent is not constant, with the series exhibiting a monotonic decrease as the fluctuation order $q$ increases. This behavior is clearly depicted in the left panel of Fig. 6(a). The multifractal behavior becomes more pronounced for higher and positive orders of the fluctuation function, specifically $q > 2$,

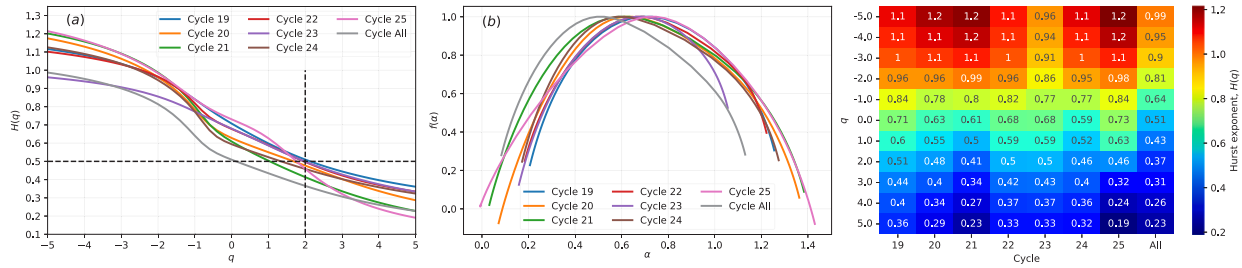


**Fig. 6.** Left panel (a) Generalized Hurst exponent $H(q)$ obtained from the MFDFA method for the series considered. Right panel (b) Correspondent spectral functions $f(\alpha)$ obtained from the MFDFA method.

indicating that all the considered series are undoubtedly antipersistent. This suggests that linear approaches may not be suitable for prediction and forecasting purposes when dealing with these phenomena.

$H$ values provide valuable insights into the correlation structure and fractality of Forbush event magnitudes across different $q$ exponents and over multiple solar cycles. For $q$ values less than 0 ($q < 0$), $H$ tends to be greater than 0.5 in most cases, suggesting long-term dependence in the data when considering lower magnitude FDs. This dependence could be related to the chaotic nature of time series, where small changes in Forbush events can influence future events. As $q$ increases and approaches 0 and positive values ($q > 0$), $H$ values decrease, approaching 0.5. This indicates weaker correlation relationships in the data, implying greater randomness or reduced long-term dependence when considering higher magnitude Forbush events.

Variability in $H$ values is observed among different solar cycles and for different $q$ values. This variability may be linked to differences in solar activity and the characteristics of Forbush events within each cycle. Cycles with lower H values may exhibit weaker correlation structures, thus implying less long-term dependence in the magnitudes of Forbush events. In the series that combines all solar cycles, there is a general trend towards $H$ values close to 0.5, especially for $q$ values near 0. This suggests that, overall, the combined Forbush event series tends to have a random walk structure or weak correlation in its data. However, differences are still observed for $q$ values further from 0, indicating patterns of long-term dependence based on event magnitude.

From Fig. 5, solar cycles 20, 21 and 24 tend to exhibit lower $H$ values compared to other cycles for most $q$ values. This suggests greater long-term dependence in the magnitudes of Forbush events during these specific solar periods, implying higher chaos or complexity in the dynamics of these events during those particular solar periods. For these cycles, with values of $H$ varying significantly for different values of $q$ indicate multifractality. This means that the correlation structure of the series changes as the scale changes, suggesting more complex and less predictable behavior. In fact, for these cycles the magnitudes are slightly smaller than for the other solar cycles as suggested in Fig. 1.

Conversely, solar cycles 19, 20 and 23 tend to show higher $H$ values for various $q$ values, implying reduced long-term dependence in their Forbush event magnitudes. This could be interpreted as greater stability or regularity in the patterns of Forbush events during these specific solar cycles. Solar cycles 21 and 24 also shown more variability in their $H$ values depending on the $q$ value. This suggests a more complex dynamic where long-term dependence varies depending on the magnitude of Forbush events and how $q$ is calculated. Precisely for this reason, they tend to be less predictable and potentially more chaotic, as the correlation structure changes considerably at different time scales.

The multifractal spectrum serves as a key indicator in the multifractal analysis of time series data, providing a quantitative measure of the level of multifractality exhibited by the series. Fig. 6(b) displays the multifractal spectra derived from our analysis. In most instances, the multifractal spectra $f(\alpha)$ exhibit stability and a parabolic shape. We observe no consistent variations between the spectral functions obtained from the combined series of all solar cycles and those derived from each individual cycle. However, it is worth noting that, except for the series corresponding to cycle 25, there is a rightward tail, contrary to all other cycles and the complete series where the tail is on the left side. This finding complements the observations regarding the $H(q)$ spectra, where the multifractal spectra obtained from the series, in general, exhibit a leftward bias (see Fig. 6(b)).

The asymmetry observed in the $f(\alpha)$ spectrum suggests the presence of distinct regimes at different scales within the multifractal spectrum. Left-sided asymmetry indicates strong multifractality at larger fluctuations, while right-sided asymmetry indicates the existence of smaller fluctuations at larger scales. Our analysis reveals that this phenomenon is present in all solar cycles and the complete series, with the exception of cycle 25, where limited data may be a contributing factor due to the cycle still being in progress. This implies that long-term temporal correlations are primarily influenced by fluctuations at large scales. Consequently, our findings suggest that the presence of multifractality in the data is predominantly driven by the underlying probability distribution function of the values, with large-scale fluctuations playing a significant role.

### 3.2. Forbush decrease and geomagnetic storm conditions

Regarding the evidence linking FD magnitudes to certain geomagnetic activity indices [19,32], and as mentioned in the section describing the data used in this study, we conducted an additional analysis on a partition of the series, focusing solely on events coinciding with geomagnetic storm conditions as measured by the $Kp_{max}$ index. After analyzing the distributions of FD magnitudes and $Kp_{max}$ indices (see Fig. 8), we defined three non-overlapping intervals, resulting in three separate series. Fig. 7 shows the three time series considered here. It is important to note that these series comprise all historical data in all solar cycles without making specific partitioning as in the previous case.

The existence of a relationship between the FD magnitude and $Kp$ index is evident. Based on the data's behavior, we modeled the relationship between the magnitude of FD events and the maximum $Kp$ index as an exponential function. The model is represented by the equation: FD magnitude $= ae^{b(Kp_{max})^{1.7}}$, with $a = 0.44 \pm 2.92 \times 10^{-5}$ and $b = -0.1 \pm 8.36 \times 10^{-7}$.

In the context of three distinct geomagnetic conditions categorized as $0 < Kp < 3$, $3 < Kp < 6$, and $6 < Kp < 9$, our analysis focused on three separate time series pertaining to FD magnitudes. Notably, the skewness and kurtosis parameters (See Fig. 9) exhibited intriguing behaviors across these conditions. For the $0 < Kp < 3$ condition, we observed that neither skewness nor kurtosis remained constant within the time scale intervals; instead, they displayed erratic variations. This unpredictability underscores the complex nature of geomagnetic dynamics within this range. Conversely, the other two conditions ($3 < Kp < 6$ and $6 < Kp < 9$) displayed a distinct and more monotonous trend as we considered larger time scales. However, as the time scales grew even larger, this previously discernible pattern dissolved, giving way to a more erratic behavior. This observation highlights the intricate interplay between geomagnetic conditions and the temporal dynamics of FD magnitude series, revealing that the behavior of skewness and

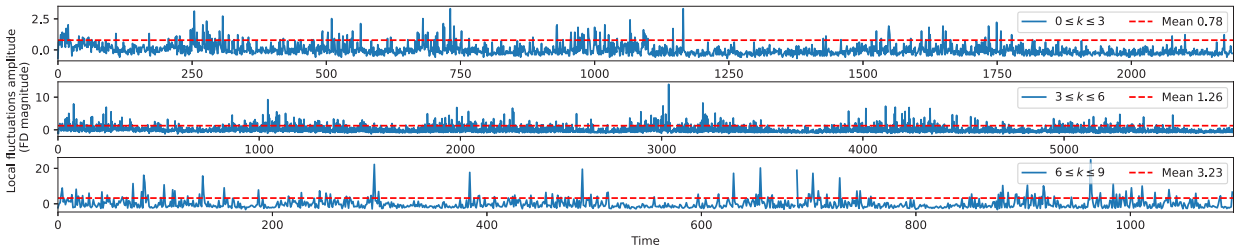


**Fig. 7.** Plots of local fluctuations amplitude for the FD magnitude considered in this study for all solar cycles but for different ranges of $K_p$ index.

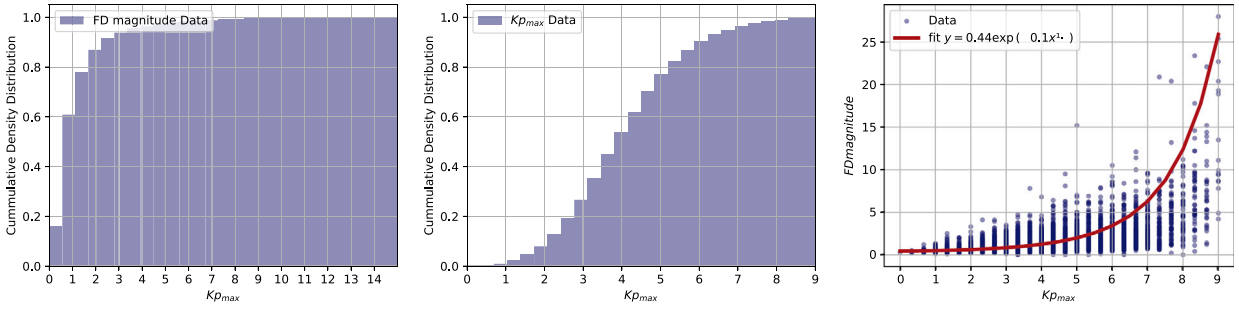


**Fig. 8.** Dependence of the mean Forbush effect magnitude on the $Kp$-index maximum of an associated magnetic storm.

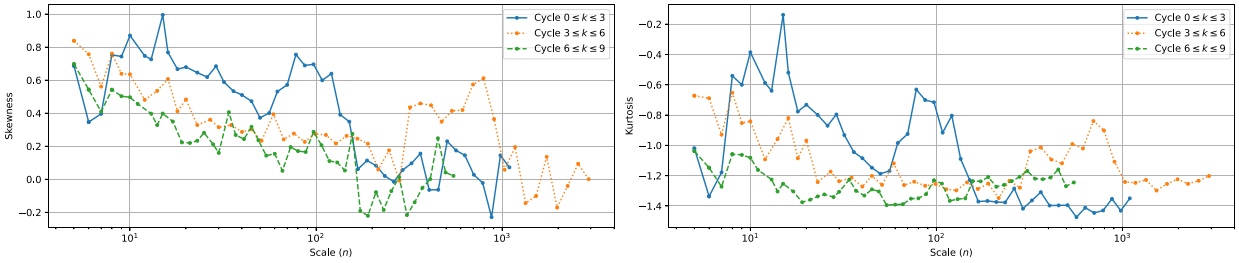


**Fig. 9.** Kurtosis and skewness parameter calculated in 30 increment scales to time-series for three different conditions in $Kp$ geomagnetic index.

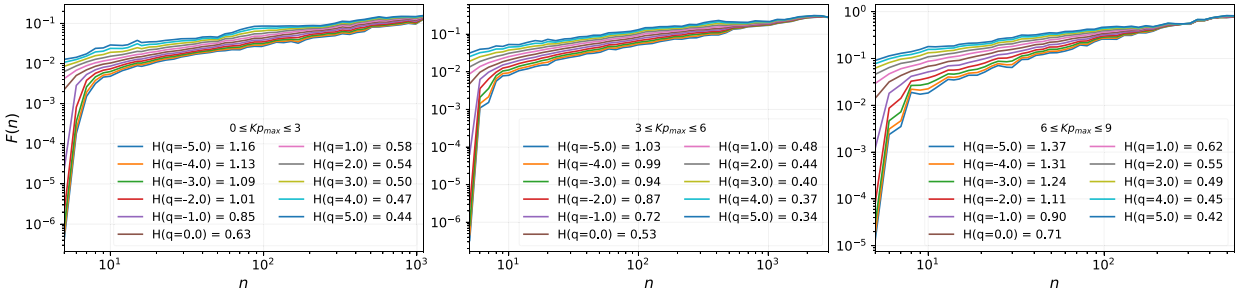


**Fig. 10.** Fluctuation function for several values of the order $q$. Fluctuation function exhibit multifractal behavior with scaling properties for several conditions of geomagnetic storm.

kurtosis is far from static and evolves in a nuanced manner, influenced by the specific geomagnetic conditions.

In this work, the $0 < Kp < 3$ filtered data showed an increase of the kurtosis parameter. In the present work, this result shows that the intermittence and coherent structures are present in the large scales of the time-series

The lengths of the three considered series are summarized in Table 1, with the series for events having a maximum $Kp$ index between 3 and 6 being the longest. For the MFDFA analysis, we employed observation windows ranging from 5 to len(data)/5, similar to the previous case. The graphical representation of the MFDFA results can be observed in Fig. 10. Consistent with the previous analysis, all series exhibit multifractal behavior at different observation scales.

Similar to the previous case, the Hurst exponent in the magnitude series of FD events does not remain constant and exhibits a monotonic decrease for values greater than $q$. However, for magnitudes of FD events corresponding to maximum $Kp$ index values between 3 and 6, the series demonstrates a much stronger fractal nature. Specifically, for values of $q > 0$, the series exhibits significantly higher antipersistence compared to the other two series. Generally, antipersistence is most evident in this latter series, followed by the series corresponding to maximum $Kp$ index ranges between 0 and 3 (representing quiet geomagnetic conditions), and finally, the series associated with more severe geomagnetic conditions displays a higher level of persistence (refer to Fig. 11(a)).

Furthermore, the multifractal spectrum differs from that of the complete FD series. Since the spectra are generally non-symmetric and

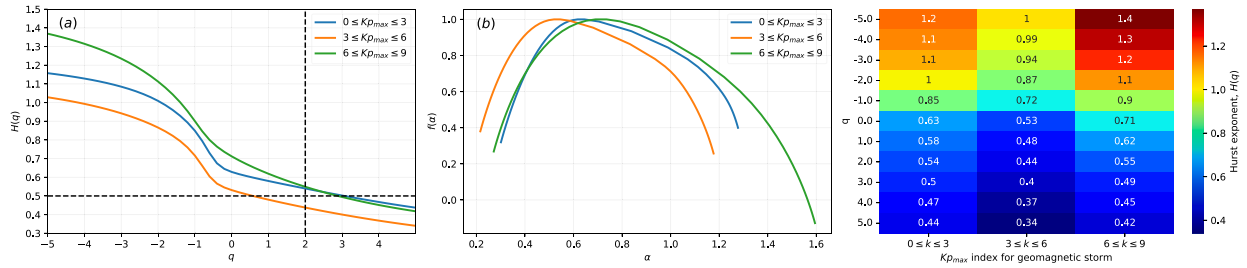


**Fig. 11.** Left panel (a): Generalized Hurst exponent $H(q)$ obtained from the MFDFA method for the series considered for several conditions of geomagnetic storm. Right panel (b): Correspondent spectral functions $f(\alpha)$ obtained from the MFDFA method for several conditions of geomagnetic storm.

skewed to the right, the geomagnetic conditions have an impact on the fractality and variability at smaller scales. This distinction is evident for both the full series and the series pertaining to quiet geomagnetic storm conditions (see Fig. 11(b)).

In general, the width of the multifractal spectrum is larger for the series that exclusively includes events with a $Kp$ index greater than 6 compared to other events with different geomagnetic conditions. Specifically, it is 37% wider than any other event and 25% wider than the full series of FD event magnitudes. This finding suggests that geomagnetic storm conditions significantly influence the fractality and variability of the series pertaining to the magnitudes of FD effects.

It is crucial to consider the size of a time series, i.e., the number of records, as it can have a substantial impact on multifractal estimates [62–65]. Even shorter time series can produce misleading outcomes in identifying multifractality. The influence of time series size on multifractal variable estimates, often referred to as size effects, has been recently explored, particularly in the context of MFDFA analysis [63,66–68].

### 3.3. Results for GHE approach application

Inspired by the observation that the sampling properties of the Hurst exponent estimation methods change with the presence of heavy tails and that in conclusion as shown in J. Barunik and L. Kristoufek (2010) [69] (also see J. Mielniczuk and P. Wojdyłło (2007) [70]), GHE provides the lowest variance and bias compared to the other methods regardless of the presence of heavy tails in the data, in the present section the calculation of the Hurst exponent is performed again.

To complement the analysis in the previous section for the determination of the Hurst exponent for the time series of intensity and magnitude of Forbush events also depending on the geomagnetic disturbance conditions and in differentiation of each solar cycle, in this section the same analysis is done but using a different methodology. In this case we consider complementing by calculating the Hurst exponent through the generalized Hurst exponent approach.

Considering exactly the same series of events we find that the Hurst exponents, although they keep the same shape and behavior, on the basis of this technique the results show some variations. Fig. 12 shows the comparison between the Hurst exponents using MFDFA and GHE, respectively.

As can be seen, although both approaches have similar distributions of Hurst exponents for different values of the $q$ parameter, when considering the time series of all solar cycles (long signal > 8000 sample points) the Hurst exponents calculated by MFDFA appear to be underestimated relative to the GHE approach. The opposite situation occurs in cycle 19 and 25 (~960 and ~270 sample points, respectively, due to the incompleteness of the cycle, this is a cycle still in process), in which the Hurst exponent values by GHE are lower than those calculated from MFDFA. For the other series (cycles 20 to 24) there are also some differences, although less notable than in the previous cases (see Fig. 13).

Regarding the time series involving the magnitudes of Forbush Decrease events under different geomagnetic distortion conditions, the differences are more significant, especially under conditions of $0 \leq Kp_{max} \leq 3$ (~2000 sample points) and $6 \leq Kp_{max} \leq 9$ (~1000 sample points). In all cases, however, the conditions of antipersistent processes for $q \geq 2$ are maintained for the two different approaches to calculating the Hurst exponent. The notable variations arise because the GHE is more sensitive to short-range perturbations compared to MFDFA [59,60].

### 3.4. More in correlation between FD magnitude and geomagnetic distortion conditions

To illustrate the necessity of discussing the multifractal properties at multiple scales, and to complement the results of the correlations between FD magnitude and $K_p$ index in previous section, we provide a MFDCCA result between these time series. It is observed the trend of $H_{ab}(q)$ with $q$ at small scales and large scales respectively instead of the whole scales. Fig. 14 (first panel on the left) shows the log–log plots of $\log F(n)$ versus $\log n$ between FD magnitude and $K_p$ index from their opening date to the total length of the series. The curves correspond to $q$ between −5 (bottom) an 5 (up). For different $q$ from −5 to 5, each curve is linear, suggesting that power-law cross-correlations exist between the two variables. As a reason that the slopes of the log–log fits to the family of $F(n)$ curves determine the Hurst exponents $H_{ab}(q)$. Then the details of the fitting procedure are crucial to the final results. The plots of $F(n)$ often show substantial fluctuations, however, in the study of solar dynamic events, this kind of situation is not to hard to find out. Just as Fig. 14 shows, each curve approaches to a straight line. As a consequence, the Hurst exponents are constant or very close when the time scales $s$ vary in the whole range of scales.

Although we generally find multifractality due to a non-constant value of $H_{ab}(q)$ in the correlation of the considered series, the values of $H_{ab}(q)$ in Fig. 14 (central panel) are all close to zero. Therefore, we can conclude that these are correlations for antipersistent processes, and this antipersistence is maintained across virtually all scales $n$, but not in an extreme way. This range indicates a moderate tendency towards reversal of the direction of fluctuations, but without strong antipersistence.

The symmetry of the $f(\alpha)$ curve refers to how the multifractal partition function responds to changes in the direction of fluctuations (positive or negative) in the correlations of the time series. In this case in which the curve $f(\alpha)$ is perfectly symmetric around the central point ($\alpha = 0$), it indicates a completely symmetric distribution of fluctuations in the correlations of the time series. This could imply that positive and negative fluctuations have a balanced distribution. Given this more complex symmetry that may indicate a combination of persistence and antipersistence on different time scales, there may be specific regions where positive or negative correlations predominate.

Finally, the empirical results obtained through MFDCCA method infer the existence of multifractal cross-correlations on the bivariate time series considered.

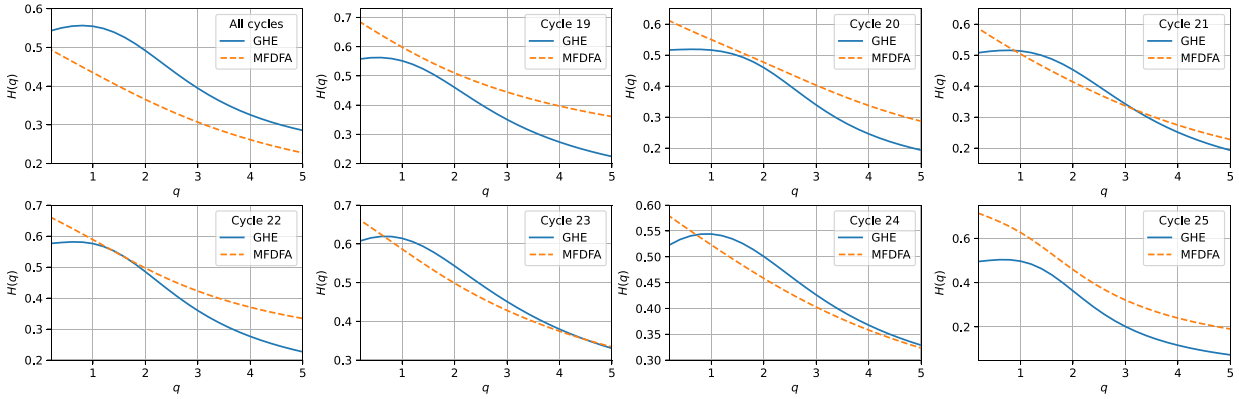


**Fig. 12.** Comparison of the Hurst exponents for $q > 0$ using the MFDFA and GHE method, respectively, for the time series of Forbush Decrease magnitudes in each solar cycle considered and also in the time series of all complete solar cycles.

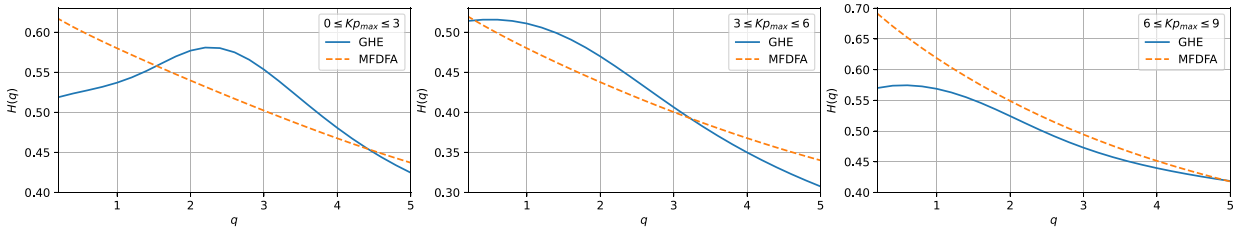


**Fig. 13.** Comparison of the Hurst exponents for $q > 0$ using the MFDFA and GHE method, respectively, for the time series of Forbush Decrease magnitudes in different geomagnetic distortion conditions.

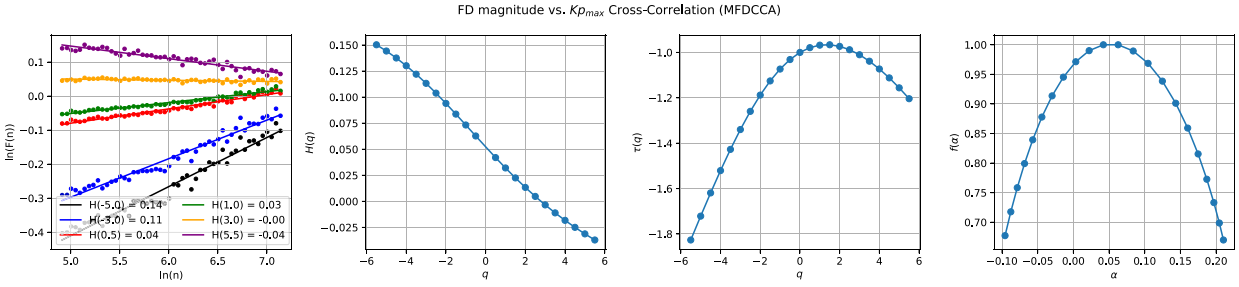


**Fig. 14.** The log–log plots of $F(n)$ versus $n$ between FD magnitude and $K_p$ index from their opening date to the total length of the series. The curves correspond to $q$ between −5 (bottom) an 5 (up).

## 4. Implications of time series analysis techniques in explaining solar physics phenomena

The application of time series analysis techniques in the field of solar physics has provided crucial insights into understanding the dynamic behavior of the Sun and its profound influence on space weather. In this section, we delve into the implications of employing these methodologies, with a focus on the urgent need for predicting extreme solar events, comprehending space weather dynamics, and discerning solar conditions that affect our climate and technology.

Recent studies, concerning to advancing in Solar Flare prediction, such as the work by Leka et al. (See for example [71–74]), have harnessed advanced time series analysis methods to enhance the prediction of solar flares. Machine learning algorithms combined with time series data have demonstrated promising results in forecasting solar flare occurrence, addressing the critical requirement for space weather forecasting and safeguarding technological assets.

Additionally, the implications of time series analysis extend to the protection of critical infrastructure against solar-induced disruptions. Some research underscores the importance of space weather forecasting based on time series analysis to mitigate the potential impact on power grids, satellite communications, and GPS systems. These advancements are essential for ensuring the resilience of modern technology [75, 76]. Time series analysis techniques have played a pivotal role in unraveling the intricate connections between solar activity and terrestrial phenomena. Recent investigations, as exemplified by several authors [77,78], have employed wavelet analysis to explore the solar influence on climate variability. These insights are critical for deciphering solar-induced climatic changes and their implications for Earth's environment.

The precise prediction of solar cycles and their impact on climate is of paramount importance. In debt to time series analysis, researchers, have made significant strides in forecasting the amplitude and duration of solar cycles. These forecasts are crucial for climate studies, as they inform our understanding of long-term climate variability. Time series analysis techniques have emerged as indispensable tools for unraveling solar physics phenomena and addressing pressing challenges in space weather prediction, critical infrastructure protection, and climate studies.

## 5. Concluding remarks

In conclusion, the study analyzed Forbush Decrease (FD) events in different solar cycles and investigated their relationship with geomagnetic storm conditions. The analysis included a total of 8216 FD events from 1957 to 2021, spanning six solar cycles (Cycle 19 to Cycle 25).

The seasonal behavior of solar activity, as observed in sunspots, was found to have a less pronounced effect on the magnitudes of FD events. The fluctuation function analysis using the Multifractal Detrended Fluctuation Analysis (MFDFA) method revealed multifractal behavior at different observation scales for all solar cycles and the complete 65-year series. The fluctuation function exhibited larger fluctuations for larger window sizes and smaller variations for smaller time scales. The Hurst exponent, which characterizes long-term temporal correlations, was found to be decreasing as the fluctuation order increased, indicating antipersistent behavior for higher-order fluctuations.

The multifractal spectra obtained from the analysis showed stability and parabolic shape in most cases. However, Cycle 25 exhibited a slightly different behavior, potentially due to the limited data available since the cycle was still ongoing. The spectra displayed an asymmetry, with a left-sided tail in all solar cycles except Cycle 25, suggesting the presence of strong multifractality at larger fluctuations and smaller fluctuations at larger scales. The analysis indicated that long-range temporal correlations were mainly influenced by large-scale fluctuations.

Furthermore, the study explored the correlation between FD magnitudes and geomagnetic storm conditions measured by the $Kp_{max}$ index. A partition of the data was created to focus on FD events occurring during geomagnetic storm conditions. The analysis revealed a relationship between FD magnitudes and the maximum $Kp$ index, which was modeled as an exponential function. The series corresponding to different geomagnetic storm conditions exhibited multifractal behavior, with the series associated with more severe geomagnetic conditions displaying higher antipersistence.

The multifractal spectra for the series under different geomagnetic storm conditions showed variations compared to the complete FD series. The spectra were generally non-symmetric and skewed to the right, indicating an influence of geomagnetic conditions on fractality and variability at small scales. The width of the multifractal spectrum was largest for the series including events with a maximum $Kp$ index greater than 6, indicating a strong influence of geomagnetic storm conditions on the fractality and variability of FD magnitudes.

In summary, this study provided insights into the multifractal properties of FD events in different solar cycles and their association with geomagnetic storm conditions. The findings highlighted the complex nature of FD magnitudes and their dependence on solar and geomagnetic activity, contributing to a better understanding of space weather phenomena.

In a future work we intend to perform a more exhaustive study adding some other indices for FD events, as well as, the analysis of the event duration itself, i.e., using the data of cosmic ray counts measured by neutron monitors at different lengths (adding the geomagnetic rigidity cutoff effect) instead of analyzing the magnitude of the events as such.

## CRediT authorship contribution statement

**D. Sierra-Porta:** Conceptualization, Data curation, Formal analysis, Investigation, Methodology, Software, Validation, Visualization, Writing – original draft, Writing – review & editing.

## Declaration of competing interest

The authors declare that they have no known competing financial interests or personal relationships that could have appeared to influence the work reported in this paper.

## Data availability

Data will be made available on request.

## Acknowledgments

DSP is deeply grateful to the reviewers for their valuable comments and suggestions to enrich the work. Additionally, we thank the UTB Research Direction for the unconditional support provided during the development of this research. This research did not receive any financial support or funding from any organization or institution. However, DSP thanks UTB for providing the computing equipment necessary for achieving the results of this investigation.

DSP thanks an anonymous reviewer for comments that helped improve the clarity of the article as well as suggesting some important references that I was not aware of.

## References

[1] Gabici S. Low-energy cosmic rays: regulators of the dense interstellar medium. Astron Astrophys Rev 2022;30(1):4. http://dx.doi.org/10.1007/s00159-022-00141-2.

[2] Owens MJ, Usoskin I, Lockwood M. Heliospheric modulation of galactic cosmic rays during grand solar minima: Past and future variations. Geophys Res Lett 2012;39(19). http://dx.doi.org/10.1029/2012GL053151.

[3] Zhao L-L, Qin G, Zhang M, Heber B. Modulation of galactic cosmic rays during the unusual solar minimum between cycles 23 and 24. J Geophys Res Space Phys 2014;119(3):1493–506. http://dx.doi.org/10.1002/2013JA019550.

[4] Forbush SE. On the effects in cosmic-ray intensity observed during the recent magnetic storm. Phys Rev 1937;51(12):1108. http://dx.doi.org/10.1103/PhysRev.51.1108.3.

[5] Forbush S. On cosmic-ray effects associated with magnetic storms. Terr Magn Atmos Electr 1938;43(3):203–18. http://dx.doi.org/10.1029/TE043i003p00203.

[6] Forbush SE. On world-wide changes in cosmic-ray intensity. Phys Rev 1938;54(12):975. http://dx.doi.org/10.1103/PhysRev.54.975.

[7] Cho K-S, Bong S-C, Moon Y-J, Dryer M, Lee S-E, Kim K-H. An empirical relationship between coronal mass ejection initial speed and solar wind dynamic pressure. J Geophys Res Space Phys 2010;115(A10). http://dx.doi.org/10.1029/2009JA015139.

[8] Gosling J, Bame S, McComas D, Phillips J. Coronal mass ejections and large geomagnetic storms. Geophys Res Lett 1990;17(7):901–4. http://dx.doi.org/10.1029/GL017i007p00901.

[9] Lockwood JA. Forbush decreases in the cosmic radiation. Space Sci Rev 1971;12(5):658–715. http://dx.doi.org/10.1007/BF00173346.

[10] Barouch E, Burlaga L. Causes of Forbush decreases and other cosmic ray variations. J Geophys Res 1975;80(4):449–56. http://dx.doi.org/10.1029/JA080i004p00449.

[11] Iucci N, Parisi M, Storini M, Villoresi G. Forbush decreases: origin and development in the interplanetary space. Il Nuovo Cimento C 1979;2(1):1–52. http://dx.doi.org/10.1007/BF02507712.

[12] Thomas BT, Gall R. Solar-flare-induced Forbush decreases: Dependence on shock wave geometry. J Geophys Res Space Phys 1984;89(A5):2991–6. http://dx.doi.org/10.1029/JA089iA05p02991.

[13] Ifedili S. The two-step Forbush decrease: An empirical model. J Geophys Res Space Phys 2004;109(A2). http://dx.doi.org/10.1029/2002JA009814.

[14] Cane HV. Coronal mass ejections and Forbush decreases. In: Cosmic rays and earth: proceedings of an ISSI workshop, 21–26 March 1999, Bern, Switzerland. Springer; 2000, p. 55–77. http://dx.doi.org/10.1007/978-94-017-1187-6_4.

[15] Belov A, Abunin A, Abunina M, Eroshenko E, Oleneva V, Yanke V, Papaioannou A, Mavromichalaki H, Gopalswamy N, Yashiro S. Coronal mass ejections and non-recurrent Forbush decreases. Sol Phys 2014;289:3949–60. http://dx.doi.org/10.1007/s11207-014-0534-6.

[16] Richardson I, Cane H. Geoeffectiveness (Dst and Kp) of interplanetary coronal mass ejections during 1995–2009 and implications for storm forecasting. Space Weather 2011;9(7). http://dx.doi.org/10.1029/2011SW000670.

[17] Papaioannou A, Belov A, Abunina M, Eroshenko E, Abunin A, Anastasiadis A, Patsourakos S, Mavromichalaki H. Interplanetary coronal mass ejections as the driver of non-recurrent Forbush decreases. Astrophys J 2020;890(2):101. http://dx.doi.org/10.3847/1538-4357/ab6bd1.

[18] Nitta NV, Mulligan T, Kilpua EK, Lynch BJ, Mierla M, O'Kane J, Pagano P, Palmerio E, Pomoell J, Richardson IG, et al. Understanding the origins of problem geomagnetic storms associated with "stealth" coronal mass ejections. Space Sci Rev 2021;217(8):82. http://dx.doi.org/10.1007/s11214-021-00857-0.

[19] Belov A, Eroshenko E, Oleneva V, Struminsky A, Yanke V. What determines the magnitude of Forbush decreases? Adv Space Res 2001;27(3):625–30. http://dx.doi.org/10.1016/S0273-1177(01)00095-3.

[20] Smith EJ. The heliospheric current sheet and modulation of galactic cosmic rays. J Geophys Res Space Phys 1990;95(A11):18731–43. http://dx.doi.org/10.1029/JA095iA11p18731.

[21] Matzka J, Stolle C, Yamazaki Y, Bronkalla O, Morschhauser A. The geomagnetic Kp index and derived indices of geomagnetic activity. Space Weather 2021;19(5):e2020SW002641. http://dx.doi.org/10.1029/2020SW002641.

[22] Elliott HA, Jahn J-M, McComas DJ. The Kp index and solar wind speed relationship: Insights for improving space weather forecasts. Space Weather 2013;11(6):339–49. http://dx.doi.org/10.1002/swe.20053.

[23] Wanliss JA, Showalter KM. High-resolution global storm index: Dst versus SYM-H. J Geophys Res Space Phys 2006;111(A2). http://dx.doi.org/10.1029/2005JA011034.

[24] Neupert WM, Pizzo V. Solar coronal holes as sources of recurrent geomagnetic disturbances. J Geophys Res 1974;79(25):3701–9. http://dx.doi.org/10.1029/JA079i025p03701.

[25] Baker D, Li X, Turner N, Allen J, Bargatze L, Blake J, Sheldon R, Spence HE, Belian R, Reeves G, et al. Recurrent geomagnetic storms and relativistic electron enhancements in the outer magnetosphere: ISTP coordinated measurements. J Geophys Res Space Phys 1997;102(A7):14141–8. http://dx.doi.org/10.1029/97JA00565.

[26] Chertok I, Grechnev V, Belov A, Abunin A. Magnetic flux of EUV arcade and dimming regions as a relevant parameter for early diagnostics of solar eruptions–sources of non-recurrent geomagnetic storms and Forbush decreases. Sol Phys 2013;282:175–99. http://dx.doi.org/10.1007/s11207-012-0127-1.

[27] Patra SN, Ghosh K, Panja SC. Scaling and fractal dimension analysis of daily Forbush decrease data. Int J Electron Eng Res 2011;3(2):237–46.

[28] Gil A, Modzelewska R, Moskwa S, Siluszyk A, Siluszyk M, Wawrzynczak A. Indicators of space weather events in cosmic rays during the solar cycle 24. In: 36th international cosmic ray conference - ICRC2019-July 24th - August 1st, 2019 Madison, WI, U.S.A. 2010.

[29] Kozlov V. Forecasting extreme space-weather events on the basis of cosmic-ray fluctuations. Cosmic Res 2022;60(2):79–88. http://dx.doi.org/10.1134/S0010952522010063.

[30] Papailiou M, Mavromichalaki H, Belov A, Eroshenko E, Yanke V. The asymptotic longitudinal cosmic ray intensity distribution as a precursor of Forbush decreases. Sol Phys 2012;280:641–50. http://dx.doi.org/10.1007/s11207-012-9945-4.

[31] Papailiou M, Abunina M, Mavromichalaki H, Belov A, Abunin A, Eroshenko E, Yanke V. Precursory signs of large Forbush decreases. Sol Phys 2021;296(6):100. http://dx.doi.org/10.1007/s11207-021-01844-y.

[32] Dumbović M, Vršnak B, Čalogović J, Župan R. Cosmic ray modulation by different types of solar wind disturbances. Astron Astrophys 2012;538:A28. http://dx.doi.org/10.1051/0004-6361/201117710.

[33] Zhang X, Zhang G, Qiu L, Zhang B, Sun Y, Gui Z, Zhang Q. A modified multifractal detrended fluctuation analysis (MFDFA) approach for multifractal analysis of precipitation in dongting lake basin, China. Water 2019;11(5):891. http://dx.doi.org/10.3390/w11050891.

[34] Zhang L, Li H, Liu D, Fu Q, Li M, Faiz MA, Ali S, Khan MI, Li T. Application of an improved multifractal detrended fluctuation analysis approach for estimation of the complexity of daily precipitation. Int J Climatol 2021;41(9):4653–71. http://dx.doi.org/10.1002/joc.7092.

[35] Chakraborty S, Chattopadhyay S. Exploring the Indian summer monsoon rainfall through multifractal detrended fluctuation analysis and the principle of entropy maximization. Earth Sci Inform 2021;14(3):1571–7. http://dx.doi.org/10.1007/s12145-021-00641-2.

[36] Stavroyiannis S, Babalos V, Bekiros S, Lahmiri S, Uddin GS. The high frequency multifractal properties of bitcoin. Phys A 2019;520:62–71. http://dx.doi.org/10.1016/j.physa.2018.12.037.

[37] Zhang X, Yang L, Zhu Y. Analysis of multifractal characterization of bitcoin market based on multifractal detrended fluctuation analysis. Phys A 2019;523:973–83. http://dx.doi.org/10.1016/j.physa.2019.04.149.

[38] Miloş LR, Haţiegan C, Miloş MC, Barna FM, Boţoc C. Multifractal detrended fluctuation analysis (MF-DFA) of stock market indexes. Empirical evidence from seven central and eastern European markets. Sustainability 2020;12(2):535. http://dx.doi.org/10.3390/su12020535.

[39] Gu R, Chen H, Wang Y. Multifractal analysis on international crude oil markets based on the multifractal detrended fluctuation analysis. Phys A 2010;389(14):2805–15. http://dx.doi.org/10.1016/j.physa.2010.03.003.

[40] Yang L, Zhu Y, Wang Y. Multifractal characterization of energy stocks in China: A multifractal detrended fluctuation analysis. Phys A 2016;451:357–65. http://dx.doi.org/10.1016/j.physa.2016.01.100.

[41] Fuwape I, Ogunjo S, Akinsusi J, Rabiu B, Jenkins G. Multifractal detrended fluctuation analysis of particulate matter and atmospheric variables at different time scales. Meteorol Atmos Phys 2023;135(3):27. http://dx.doi.org/10.1007/s00703-023-00971-4.

[42] Shang P, Lu Y, Kamae S. Detecting long-range correlations of traffic time series with multifractal detrended fluctuation analysis. Chaos Solitons Fractals 2008;36(1):82–90. http://dx.doi.org/10.1016/j.chaos.2006.06.019.

[43] Zhao X, Shang P, Lin A, Chen G. Multifractal Fourier detrended cross-correlation analysis of traffic signals. Phys A 2011;390(21–22):3670–8. http://dx.doi.org/10.1016/j.physa.2011.06.018.

[44] Movahed MS, Jafari G, Ghasemi F, Rahvar S, Tabar MRR. Multifractal detrended fluctuation analysis of sunspot time series. J Stat Mech Theory Exp 2006;2006(02):P02003. http://dx.doi.org/10.1088/1742-5468/2006/02/P02003.

[45] Hu J, Gao J, Wang X. Multifractal analysis of sunspot time series: the effects of the 11-year cycle and Fourier truncation. J Stat Mech Theory Exp 2009;2009(02):P02066. http://dx.doi.org/10.1088/1742-5468/2009/02/P02066.

[46] Sierra-Porta D, Domínguez-Monterroza A-R. Linking cosmic ray intensities to cutoff rigidity through multifractal detrented fluctuation analysis. Phys A 2022;607:128159. http://dx.doi.org/10.1016/j.physa.2022.128159.

[47] Christodoulakis J, Varotsos C, Mavromichalaki H, Efstathiou M, Gerontidou M. On the link between atmospheric cloud parameters and cosmic rays. J Atmos Sol-Terr Phys 2019;189:98–106. http://dx.doi.org/10.1016/j.jastp.2019.04.012.

[48] Sierra-Porta D. On the fractal properties of cosmic rays and sun dynamics cross-correlations. Astrophys Space Sci 2022;367(12):1–14. http://dx.doi.org/10.1007/s10509-022-04151-5.

[49] Echeverría S, Moya PS, Pastén D. On the multifractality of plasma turbulence in the solar wind. Proc Int Astron Union 2019;15(S354):371–4. http://dx.doi.org/10.1017/S1743921320000514.

[50] Kasde SK, Sondhiya DK, Gwal AK. Multifractal detrended fluctuation analysis of solar wind parameters during solar cycle 23. In: 42nd COSPAR scientific assembly. Vol. 42, 2018, p. E2–3, url:https://www.cospar-assembly.org/abstractcd/COSPAR-18/abstracts/E2.3-0042-18.pdf.

[51] Babu SS, Unnikrishnan K. Analysis of fractal properties of horizontal component of earth's magnetic field of different geomagnetic conditions using MFDFA. Adv Space Res 2023. http://dx.doi.org/10.1016/j.asr.2023.05.052.

[52] Kantelhardt JW, Zschiegner SA, Koscielny-Bunde E, Havlin S, Bunde A, Stanley HE. Multifractal detrended fluctuation analysis of nonstationary time series. Phys A 2002;316(1–4):87–114. http://dx.doi.org/10.1016/S0378-4371(02)01383-3.

[53] Peng C-K, Buldyrev SV, Havlin S, Simons M, Stanley HE, Goldberger AL. Mosaic organization of DNA nucleotides. Phys Rev E 1994;49(2):1685. http://dx.doi.org/10.1103/PhysRevE.49.1685.

[54] Ossadnik S, Buldyrev S, Goldberger A, Havlin S, Mantegna R, Peng C, Simons M, Stanley H. Correlation approach to identify coding regions in DNA sequences. Biophys J 1994;67(1):64–70. http://dx.doi.org/10.1016/S0006-3495(94)80455-2.

[55] Zhou W-X, et al. Multifractal detrended cross-correlation analysis for two nonstationary signals. Phys Rev E 2008;77(6):066211. http://dx.doi.org/10.1103/PhysRevE.77.066211.

[56] Jiang Z-Q, Zhou W-X, et al. Multifractal detrending moving-average cross-correlation analysis. Phys Rev E 2011;84(1):016106. http://dx.doi.org/10.1103/PhysRevE.84.016106.

[57] Kristoufek L. Multifractal height cross-correlation analysis: A new method for analyzing long-range cross-correlations. Europhys Lett 2011;95(6):68001. http://dx.doi.org/10.1209/0295-5075/95/68001.

[58] Hedayatifar L, Vahabi M, Jafari G. Coupling detrended fluctuation analysis for analyzing coupled nonstationary signals. Phys Rev E 2011;84(2):021138. http://dx.doi.org/10.1103/PhysRevE.84.021138.

[59] Di Matteo T, Aste T, Dacorogna MM. Scaling behaviors in differently developed markets. Physica A 2003;324(1–2):183–8. http://dx.doi.org/10.1016/S0378-4371(02)01996-9.

[60] Di Matteo T, Aste T, Dacorogna MM. Long-term memories of developed and emerging markets: Using the scaling analysis to characterize their stage of development. J Bank Finance 2005;29(4):827–51. http://dx.doi.org/10.1016/j.jbankfin.2004.08.004.

[61] Di Matteo T. Multi-scaling in finance. Quant Finance 2007;7(1):21–36. http://dx.doi.org/10.1080/14697680600969727.

[62] Pamuła G, Grech D. Influence of the maximal fluctuation moment order q on multifractal records normalized by finite-size effects. Europhys Lett 2014;105(5):50004. http://dx.doi.org/10.1209/0295-5075/105/50004.

[63] Grech D, Pamuła G. On the multifractal effects generated by monofractal signals. Phys A 2013;392(23):5845–64. http://dx.doi.org/10.1016/j.physa.2013.07.045.

[64] López JL, Contreras JG. Performance of multifractal detrended fluctuation analysis on short time series. Phys Rev E 2013;87(2):022918. http://dx.doi.org/10.1103/PhysRevE.87.022918.

[65] Drożdż S, Kwapień J, Oświecimka P, Rak R. Quantitative features of multifractal subtleties in time series. Europhys Lett 2010;88(6):60003. http://dx.doi.org/10.1209/0295-5075/88/60003.

[66] Dong Q, Wang Y, Li P. Multifractal behavior of an air pollutant time series and the relevance to the predictability. Environ Pollut 2017;222:444–57. http://dx.doi.org/10.1016/j.envpol.2016.11.090.

[67] Grech D, Pamuła G. Multifractal background noise of monofractal signals. Acta Phys Pol A 2012;121(2B). doi:https://bibliotekanauki.pl/articles/1408977.pdf.

[68] Rak R, Grech D. Quantitative approach to multifractality induced by correlations and broad distribution of data. Phys A 2018;508:48–66. http://dx.doi.org/10.1016/j.physa.2018.05.059.

[69] Barunik J, Kristoufek L. On hurst exponent estimation under heavy-tailed distributions. Physica A 2010;389(18):3844–55. http://dx.doi.org/10.1016/j.physa.2010.05.025.

[70] Mielniczuk J, Wojdyłło P. Estimation of hurst exponent revisited. Comput Stat Data Anal 2007;51(9):4510–25. http://dx.doi.org/10.1016/j.csda.2006.07.033.

[71] Barnes G, Leka K, Schrijver C, Colak T, Qahwaji R, Ashamari O, Yuan Y, Zhang J, McAteer R, Bloomfield D, et al. A comparison of flare forecasting methods. I. Results from the "all-clear" workshop. Astrophys J 2016;829(2):89. http://dx.doi.org/10.3847/0004-637X/829/2/89.

[72] Leka K, Park S-H, Kusano K, Andries J, Barnes G, Bingham S, Bloomfield DS, McCloskey AE, Delouille V, Falconer D, et al. A comparison of flare forecasting methods. II. Benchmarks, metrics, and performance results for operational solar flare forecasting systems. Astrophys J Suppl Ser 2019;243(2):36. http://dx.doi.org/10.3847/1538-4365/ab2e12.

[73] Leka K, Park S-H, Kusano K, Andries J, Barnes G, Bingham S, Bloomfield DS, McCloskey AE, Delouille V, Falconer D, et al. A comparison of flare forecasting methods. III. Systematic behaviors of operational solar flare forecasting systems. Astrophys J 2019;881(2):101. http://dx.doi.org/10.3847/1538-4357/ab2e11.

[74] Park S-H, Leka K, Kusano K, Andries J, Barnes G, Bingham S, Bloomfield DS, McCloskey AE, Delouille V, Falconer D, et al. A comparison of flare forecasting methods. IV. Evaluating consecutive-day forecasting patterns. Astrophys J 2020;890(2):124. http://dx.doi.org/10.3847/1538-4357/ab65f0.

[75] Ledvina VE, Palmerio E, McGranaghan RM, Halford AJ, Thayer A, Brandt L, MacDonald EA, Bhaskar A, Dong C, Altintas I, et al. How open data and interdisciplinary collaboration improve our understanding of space weather: A risk and resiliency perspective. Front Astron Space Sci 2022;9:1067571. http://dx.doi.org/10.3389/fspas.2022.1067571.

[76] Riley P, Baker D, Liu YD, Verronen P, Singer H, Güdel M. Extreme space weather events: From cradle to grave. Space Sci Rev 2018;214:1–24. http://dx.doi.org/10.1007/s11214-017-0456-3.

[77] Tsurutani BT, Lakhina GS, Hajra R. The physics of space weather/solar-terrestrial physics (STP): what we know now and what the current and future challenges are. Nonlinear Process Geophys 2020;27(1):75–119. http://dx.doi.org/10.5194/npg-27-75-2020.

[78] Kusano K, Ichimoto K, Ishii M, Miyoshi Y, Yoden S, Akiyoshi H, Asai A, Ebihara Y, Fujiwara H, Goto T-N, et al. PSTEP: project for solar–terrestrial environment prediction. Earth Planets Space 2021;73:1–29. http://dx.doi.org/10.1186/s40623-021-01486-1.